MIB2 Functions in Oocyte Meiosis by Modulating Chromatin Configuration

Authors

Yifei Jin, Guangyi Sun, Jiashuo Li, Qing Cheng, Hongzheng Sun, Longsen Han, Xuejiang Guo, Shuai Zhu, and Qiang Wang

Correspondence

zhus2018@njmu.edu.cn;
qwang2012@njmu.edu.cn

In Brief

Based on quantitative proteomics, we quantified differentially expressed proteins in GV-stage mouse oocytes (SN and NSN types). Bioinformatics analysis identified enriched pathways of these proteins and revealed elevated MIB2 in SN oocytes. Functional validation suggests that MIB2-regulated chromatin structural changes are crucial for oocyte developmental competence.

Graphical Abstract

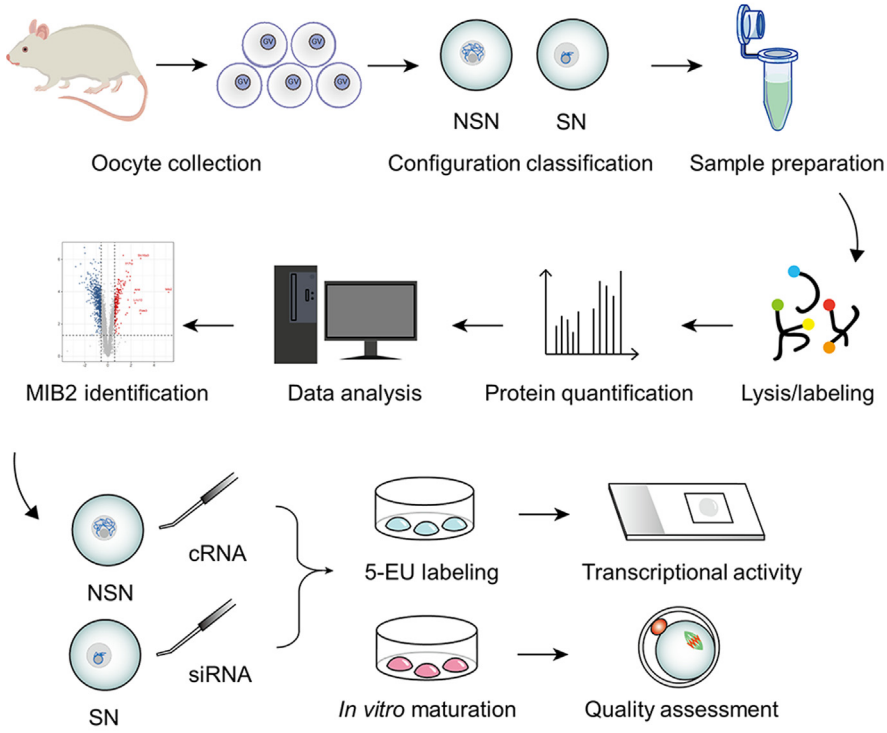

Highlights

- *In vivo* quantitative and comparative analysis performed for mouse GV stage oocytes.
- Pathways enriched by differentially expressed proteins were systematically analyzed.
- MIB2 regulates the transition of oocytes from NSN to SN type.
- MIB2 promotes oocyte meiotic maturation and early developmental competence.

2024, Mol Cell Proteomics *23*(*8*), 100813

https://doi.org/10.1016/j.mcpro.2024.100813

MIB2 Functions in Oocyte Meiosis by Modulating Chromatin Configuration

Yifei Jin[1,‡], Guangyi Sun[1,‡], Jiashuo Li[1,‡], Qing Cheng[2,‡], Hongzheng Sun[1], Longsen Han[1], Xuejiang Guo[1], Shuai Zhu[1,*], and Qiang Wang[1,3,*]

Chromatin configuration serves as a principal indicator of GV (germinal vesicle)-stage oocyte quality. However, the underlying mechanisms governing the chromatin configuration transition from NSN (non-surrounded nucleolus) to SN (surrounded nucleolus) remain unclear. In this study, by conducting a quantitative proteomic analysis, we identified an increased expression of the MIB2 (MIB E3 ubiquitin protein ligase 2) protein in SN oocytes. Specific depletion of MIB2 in SN oocytes not only leads to severe disruption of the meiotic apparatus and a higher incidence of aneuploidy but also adversely affects meiotic maturation and early embryo development. Notably, overexpression of MIB2 in NSN oocytes facilitates the chromatin configuration transition. Meantime, we observed that forced expression of MIB2 in NSN oocytes significantly mitigates spindle/chromosome disorganization and aneuploidy. In summary, our results suggest that chromatin configuration transition regulated by MIB2 is crucial for oocytes to acquire developmental competence.

Successful meiotic maturation of oocytes is the basis for healthy embryo production and female fertility (1–4). In mammals, oocytes are arrested at the diplotene stage of the first meiotic prophase, a phase also referred to as the germinal vesicle (GV) stage (5, 6). Upon stimulation by a surge of luteinizing hormone (LH) secretion from the anterior pituitary gland before ovulation, oocytes that were arrested at the GV stage resume meiosis. The nucleolus and nuclear envelope disappear, and the chromosomes condense into a compact state, a process known as germinal vesicle breakdown (GVBD). After GVBD, the oocyte progresses to metaphase I (MI), during which the chromosomes align at the metaphase plate (4). Spindle fibers attach to the centromeres, preparing for the separation of chromosomes in the following anaphase I (7). Subsequently, the oocyte enters anaphase I, accompanied by the extrusion of the first polar body. Finally, the oocyte is arrested again in metaphase II (MII) of meiosis, awaiting fertilization (8). Oocyte maturation is a crucial step in acquiring the ability for successful fertilization and subsequent embryo development (9).

During the late stages of oogenesis, large-scale chromatin remodeling is evidenced by alterations in chromatin configuration which refers to the spatial arrangement of chromatin (10, 11). GV oocytes can adopt one of two chromatin configurations: non-surrounded nucleolus (NSN) or surrounded nucleolus (SN) (12). As mouse oocytes grow and develop, their chromatin configuration undergoes a transition from NSN to SN. Oocytes from mice younger than 15 days predominantly exhibit an NSN configuration. Subsequently, a subset of oocytes undergoes a transition to the SN configuration (13). NSN oocytes feature diffuse chromatin that does not form distinct chromatin boundaries around the nucleolus. They exhibit high transcription levels and can synthesize various types of RNA. In contrast, SN oocytes display condensed chromatin, particularly localized around the nucleolus, and are in a state of global transcriptional repression (14, 15). While NSN oocytes exhibit a diminished rate of meiotic maturation and experience developmental arrest at the 2-cell stage, SN oocytes have the potential to develop into blastocysts (16–18).

It has been reported that the disparities in meiotic maturation and developmental potential between SN and NSN oocytes can be attributed to the factors present within the cytoplasm and nucleus (16). Nuclear factors associated with the NSN to SN transition include NPM2 (nuclear phosphoprotein 2), which is a nuclear factor required for establishing the SN configuration (10). Poly(rC) binding protein 1 (PCBP1), involved in maintaining transcriptional silence, increases the proportion of NSN configuration when knocked down (19). The transcriptome profile of SN oocytes shows upregulation of Oct-4 and Stella expression, contributing to the developmental potential of SN oocytes (20). Furthermore, the loss of ribosomal protein RPS26 results in a failure of the NSN-SN transition, accompanied by a decrease in transcriptional

From the [1]State Key Laboratory of Reproductive Medicine and Offspring Health, Changzhou Maternity and Child Health Care Hospital, Changzhou Medical Center, Nanjing Medical University, Nanjing, China; [2]Women's Hospital of Nanjing Medical University, Nanjing Women and Children's Healthcare Hospital, Nanjing, China; [3]Center for Global Health, School of Public Health, Nanjing Medical University, Nanjing, China

‡These authors contributed equally to this work.

*For correspondences: Qiang Wang, qwang2012@njmu.edu.cn; Shuai Zhu, zhus2018@njmu.edu.cn.

https://doi.org/10.1016/j.mcpro.2024.100813

activity, DNA, and histone methylation, ultimately leading to premature ovarian failure (21). Hence, the transition of chromatin configuration is crucial for oocytes to acquire meiotic competence and early embryo developmental potential (22), but factors contributing to developmental competence during the NSN to SN transition remain poorly understood.

In this study, through quantitative proteomic analysis of SN and NSN oocytes, we identified MIB2 (MIB E3 ubiquitin protein ligase 2) as the protein exhibiting the most significant upregulation. Utilizing knockdown and overexpression experiments, we confirmed the pivotal role of MIB2 in facilitating the transition of oocyte chromatin configuration, as well as in enhancing meiotic maturation and developmental competence.

EXPERIMENTAL PROCEDURES

Mice

Female ICR mice (3–4 weeks old) were purchased from the experimental animal center of Nanjing Medical University and were housed in ventilated cages with a standard 12 h/12 h light/dark cycle at room temperature (22 °C) under controlled humidity (20–30%). All animal work and experiments were carried out according to relevant ethical guidelines and regulations, and approved by the Animal Care and Use Committee of Nanjing Medical University (Protocol NO. IACUC-2206014).

Antibodies

Rabbit polyclonal anti-MIB2 antibody were purchased from Abcam (Cat#: A17829); Mouse monoclonal FITC conjugated anti α-tubulin antibody were purchased from Sigma (Cat#: F2168); human anti-centromere CREST antibody was purchased from Antibodies Incorporated (Cat#: 15234); Cy5-conjugated donkey anti-human IgG was purchased from Jackson Immuno-Research Laboratory (Cat#: 709605149 and 705095147); mouse monoclonal anti-Myc tag antibody were purchased from Abcam (Cat#: ab18185); and horseradish peroxidase (HRP) conjugated goat anti-rabbit IgG purchased from Protein Tech (Cat#: SA00001-2). Except for those specifically stated, all chemicals and culture media in our research were purchased from Sigma.

Collection, Classification, and Culture of Oocytes

Oocytes were retrieved from female mice at the age of 3 to 4 weeks. Cumulus cells were removed by repeated mouth pipetting. To sort for the different oocytes at GV states, oocytes were stained for 15 min with 0.1 μg/ml Hoechst 33,342 and manually sorted by exposure to UV light for ~1 s using an inverted fluorescence microscope. The nucleus showed diffuse Hoechst staining, with a few dense areas of punctated staining, classified as NSN. A fully closed perinucleolar ring of Hoechst staining in the nucleus, which were categorized as SN (23). Oocytes that could not be categorized were excluded from further experiments. For *in vitro* maturation, GV oocytes were cultured in M16 medium (Nanjing Luanchuang Co) under mineral oil at 37 °C in a 5% CO2 incubator.

Proteomics

Mouse SN and NSN oocyte samples were collected and lysed using a urea lysis buffer (8 M urea, 75 mM NaCl, 50 mM Tris, pH 8.2, 1% (v/v) EDTA-free protease inhibitor, 1 mM NaF, 1 mM beta-glycerophosphate, 1 mM sodium orthovanadate, 10 mM pyrophosphate, 1 mM PMSF). The lysates were centrifuged at 40,000*g* for 1 h. As previously described, the proteins were reduced, alkylated, and digested with trypsin. Following digestion, TMT labeling was performed according to the manufacturer's protocol. To improve protein identification and quantification coverage, mixed TMT-labeled peptides were fractionated using high-pH reversed-phase (HP-RP) separation technology based on an ACQUITY UPLC M-Class system (Waters) with a BEH C18 column (300 μm × 150 mm, 1.7 μm; water). A total of 35 fractions were collected and then lyophilized.

All fractions were reconstituted in 0.1% FA and analyzed using an Orbitrap Fusion Lumos mass spectrometer (ThermoFisher Scientific) coupled with a Proxeon Easy-nLC 1200 system. Trap column (75 μm × 2 cm, Acclaim PepMap100, Thermo) and analytical column (75 μm × 25 cm, Acclaim PepMap RSLC, Thermo) with a flow rate of 300 nl/min were operated for peptides separation under a 95-min linear gradient (3% to 5% buffer B over 5 s, 5% to 15% buffer B over 40 min, 15% to 28% buffer B over 34 min and 50 s, 28% to 38% buffer B over 12 min, 38% to 100% buffer B over 5 s, 100% buffer B for 8 min). MS parameters can be found in the previously published paper (24). In summary, data were acquired through MS1 scans in the m/z range of 350 to 1500 with a resolution of 60,000, followed by Orbitrap-related HCD MS2 spectra at a resolution of 50,000 with an HCD collision energy of 36%.

The raw files were searched against the UniProt mouse protein database using MaxQuant software (Version 1.6.5.0). Peptide and protein identifications were filtered to achieve a false discovery rate (FDR) of 1%. The precursor mass tolerance was set to 20 ppm, and the product ion mass tolerance was set to 0.5 Da. Trypsin/P enzyme specificity was used for the search, allowing for a maximum of two missed cleavages. Cysteine residue carbamidomethylation (+57.0215 Da) was set as a fixed modification. Variable modifications included methionine oxidation and protein N-terminal acetylation. For TMT-based quantification, protein quantitation values were calculated using the MaxQuant reporter ion MS2 method. Peptides and proteins with FDR ≤1% and at least one unique peptide were considered for quantitative analysis. The spectra of the single unique peptides are shown in Supplemental Fig. S1.

For the two sets of oocyte proteomics, significant differences in protein abundance between the groups were statistically analyzed using FDR-corrected t-tests. To better identify and visualize differentially expressed proteins between the groups, volcano plots, and heatmaps were constructed to depict the degree of protein expression similarity between samples. To further annotate the differentially expressed proteins, Ensemble gene IDs were used for bioinformatics analysis. Gene Ontology (GO) term pathways with FDR-q values <0.05 were considered significantly enriched. The GO enrichment analysis was performed using Pathway Studio (Version 6.00) software (Ariadne Genomics).

Plasmid Construction and cRNA Synthesis

Total RNA was extracted from 50 oocytes using the Arcturus PicoPure RNA isolation kit (KIT0204; Applied Biosystems), and cDNA generation was performed using Quantitect Reverse Transcription kit (205,311; Qiagen). Plasmid construction and cRNA synthesis were conducted as we reported previously (Zeng *et al*., 2018). Purified PCR products were digested with EcoRI and AscI (R3101S and R0588S, NEB), and then cloned into the pCS2+ vector with Myc tags. For mRNA synthesis, the plasmids were linearized by NotI and capped RNAs were produced using SP6 mMESSAGE mMACHINE (AM1340; Thermo Fisher) according to the manufacturer's instruction. Synthesized RNA was purified by Arcturus PicoPure RNA Isolation Kit (74,004; Qiagen). Synthesized cRNA was aliquoted and stored at −80 °C. The following primers were used to amplify the CDS sequence of MIB2:

forward primer, 5′- TTCTGAAGAGGACTTGAATTCAATGGACC TGGACCCCCATGCAGGT-3′,

reverse primer, 5′- CTATAGTTCTAGAGGCGCGCCTCACACGAA-GATCTGAATGCGGTCGC-3′.

Knockdown and Overexpression Experiments

A Narishige microinjector was used for knockdown and overexpression in microinjection experiments. siRNA duplexes against MIB2 was purchased from Gene Pharma and diluted to 20 μmol/L stock solutions. 2.5 pl MIB2 siRNA (1 mM) was injected into oocytes for knockdown analysis, or an equivalent amount of negative siRNA. 10 pl cRNA (10 ng/μl) was microinjected into GV oocytes for overexpression experiments. After injections, in order to hinder mRNA translation or facilitate MIB2 overexpression, oocytes were arrested at the GV stage in the M16 medium containing 2.5 μM milrinone for 10 h. And then cultured in an M16 medium without milrinone for further experiments. MIB2-siRNA primers are as follows:

forward primer, 5′- GUCGCUGUGAUGUGAAUGUTT-3′,

reverse primer, 5′- ACAUUCACAUCACAGCGACTT-3′.

Western Blotting

The samples containing a sufficient number of oocytes (at least 100) were lysed in Laemmli buffer and incubated at 95 °C for 5 min before electrophoresis. Total oocyte proteins were separated by 10% SDS-PAGE and electrophoretically transferred to the PVDF membrane. The membrane was blocked for 1 h with 5% low-fat dry milk diluted by PBST at room temperature, and incubated with appropriate primary antibodies overnight at 4 °C, followed by three washes with PBST (PBS containing 0.1% Tween 20) and incubation with HRP-conjugated secondary antibody for 1 h at room temperature. Then, the protein bands were visualized using an ECL Plus Western Blotting Detection System (GE Healthcare, Little Chalfont). Tubulin was used as a loading control.

Parthenogenetic Activation and Embryo Culture

After oocytes developed to the MII stage in M16 medium, they could be transferred to an activating medium, where oocytes were incubated for 5.5 h at 37 °C with 5% CO_2 in air. The activating medium used was a Ca^{2+}-free CZB medium (Nanjing Luanchuang Co) supplemented with 10 mM $SrCl_2$ and 5 μg/ml cytochalasin B. At the end of the activation treatment, oocytes were examined for activation under a phase contrast microscope. Oocytes containing one or two well-developed prokaryotes are considered to be activated successfully. Successfully activated oocytes were then transferred to Ca^{2+} CZB (Nanjing Luanchuang Co) for 48 h to culture oocytes (30–35 oocytes per 100 μl drop) at 37°C under a humidified atmosphere with 5% CO_2 in the air. Add glucose (5.5 mM) when embryos develop beyond 3- or 4-cell stages. The number of 2-cell embryos and blastocysts were recorded at 24 h and 96 h, respectively.

ROS Evaluation

To evaluate reactive oxygen species (ROS) levels, CM-H2DCFDA (C6827; Invitrogen) was employed. Oocytes underwent a 30-min incubation in M16 medium supplemented with 5 μM CM-H2DCFDA at 37 °C within a 5% CO2 incubator. Subsequently, the oocytes were subjected to three washes and then positioned on a live cell-imaging dish, covered with mineral oil. Without delay, fluorescent images were captured using a Zeiss Laser Scanning Confocal Microscope (LSM 710; Zeiss).

Immunofluorescence and Image Analysis

As described previously (25), oocytes were fixed with 4% paraformaldehyde in PBS (pH 7.4) for 20 min at room temperature, and permeabilized in 0.5% Triton-X 100 for 15 min at RT. Then, oocytes were blocked with 1% BSA-supplemented PBS for 1 h at RT and were subjected to indirect immunofluorescence staining by incubating with primary antibodies overnight at 4 °C. After three washes, oocytes were stained with propidium iodide (PI) for 20 min to visualize chromosomes. Finally, oocytes were transferred to microscope slides and examined under a laser scanning confocal microscope in time (LSM 700, Zeiss). Multiple images were processed and intensity measurements were conducted using ZEN software. Intensity measurements of normalized cross-sections were performed using ZEN measurement functions. Data were normalized based on the background level.

Chromosome Spread

Chromosome spread was conducted as described previously (26). To remove zona pellucida, MII oocytes were placed in Tyrode's buffer (pH 2.5) for about 30s at 37 °C. After recovery in M16 medium for 10 min, oocytes were fixed in a drop of 1% paraformaldehyde with 0.15% Triton X-100 on a glass slide. After air drying, a standard immunofluorescent staining procedure was performed as mentioned above. Kinetochores were labeled with CREST and chromosomes were stained with Hoechst 33342. The laser scanning confocal microscope was used for chromosome examination.

Transcriptional Activity Detection

Dilute EU to a 100 mM stock solution using ddH2O, then further dilute it to 1 mM. Dilute the Click-iT reaction buffer additive 10-fold using ddH2O to prepare the Click-iT cocktail (C10329; Invitrogen). Transfer oocytes to an M2 culture medium containing 1 mM EU and 2.5 μM milrinone, and incubate at 37 °C for 45 min. Subsequently, fix them at room temperature in 3.7% PFA for 15 min, followed by two washes with PBST. Next, permeabilize the oocytes at room temperature for 15 min using 0.5% Triton, and wash them twice with PBST. Incubate the oocytes in the Click-iT cocktail at room temperature in the dark for 30 min. After incubation, wash them twice with Reaction Rinse Buffer. Subsequently, stain the nuclei with Hoechst 33,342, diluted at a ratio of 1:1000 in PBST, for 15 min. Finally, mount the samples on slides and observe them using a confocal laser scanning microscope.

Experimental Design and Statistical Rationale

To identify the proteomic profiles of mouse oocytes with different chromatin configurations (SN and NSN), high-throughput proteomic analysis was conducted. Three biological replicates were used for each configuration, with 300 oocytes per sample.

Student's *t* test was employed for statistical comparison between the two groups, with results presented as mean ± SD and significance accepted at $p < 0.05$. For TMT-based quantitative proteomic data, Student's *t* test and Benjamini-Hochberg correction were utilized to control the false discovery rate (FDR). Each experiment was repeated at least three times, and unless otherwise stated, the data shown in the figures are from a representative experiment. All analyses were performed using Prism v9.0 software (GraphPad).

RESULTS

Quantitative Proteomic Analysis Unveils MIB2 Protein Accumulation in SN Oocytes

Utilizing immunofluorescence Hoechst staining, we classified GV oocytes of 3 weeks of mice into NSN and SN chromatin configuration, based on the degree of chromatin condensation and its distribution around the nucleolus. Specifically, NSN oocytes are characterized by chromatin dispersed throughout the nucleus, whereas SN oocytes

exhibit highly condensed chromatin that forms a ring-like structure around the nucleolus. Here, to identify potential regulators of chromatin configuration transition, TMT-based LC-MS/MS (Liquid Chromatography with Tandem Mass Spectrometry) analysis was conducted on NSN and SN oocytes (Fig. 1*A*).

The proteomic analysis yielded 799 proteins with differential expression (p.adjust <0.05 and fold change >1.5) between NSN and SN oocytes (Supplemental Table S1). Of these, 609 proteins were downregulated and 190 were upregulated in SN oocytes compared to NSN oocytes (Fig. 1*B*). Gene Ontology (GO) pathway enrichment analysis revealed that upregulated proteins in NSN oocytes predominantly functioned in pathways related to mRNA metabolism, processing, and post-transcriptional regulation (Fig. 1*C*). Notable among these were the transcriptional regulator SNW1 (SNW domain-containing protein 1, NSN/SN ratio = 1.85) and proteins such as HNRNPH1 (heterogeneous nuclear ribonucleoprotein H1, NSN/SN = 1.58) and FMR1 (fragile X messenger ribonucleoprotein 1, NSN/SN = 1.68), along with the m6A reader protein YTHDF1 (YTH N6-methyladenosine RNA binding protein F1, NSN/SN = 1.81). Conversely, proteins upregulated in SN oocytes were associated with cell cycle progression, meiotic nuclear division, and female gamete production, including CDK1 (cyclin-dependent kinase 1, SN/NSN = 1.87), NDC80 (NDC80 kinetochore complex component, SN/NSN = 1.87), GDF9 (growth differentiation factor 9, SN/NSN = 2.63), and BMP15 (bone morphogenetic protein 15, SN/NSN = 2.56). The documented roles of these proteins in oocyte growth and development (27–31) lend credibility to our proteomic data. Growing oocytes increase in size and accumulate factors that support later development (32). Among the upregulated proteins in SN oocytes, the one with the most significant change is the E3 ubiquitin-protein ligase MIB2 (MIB E3 ubiquitin

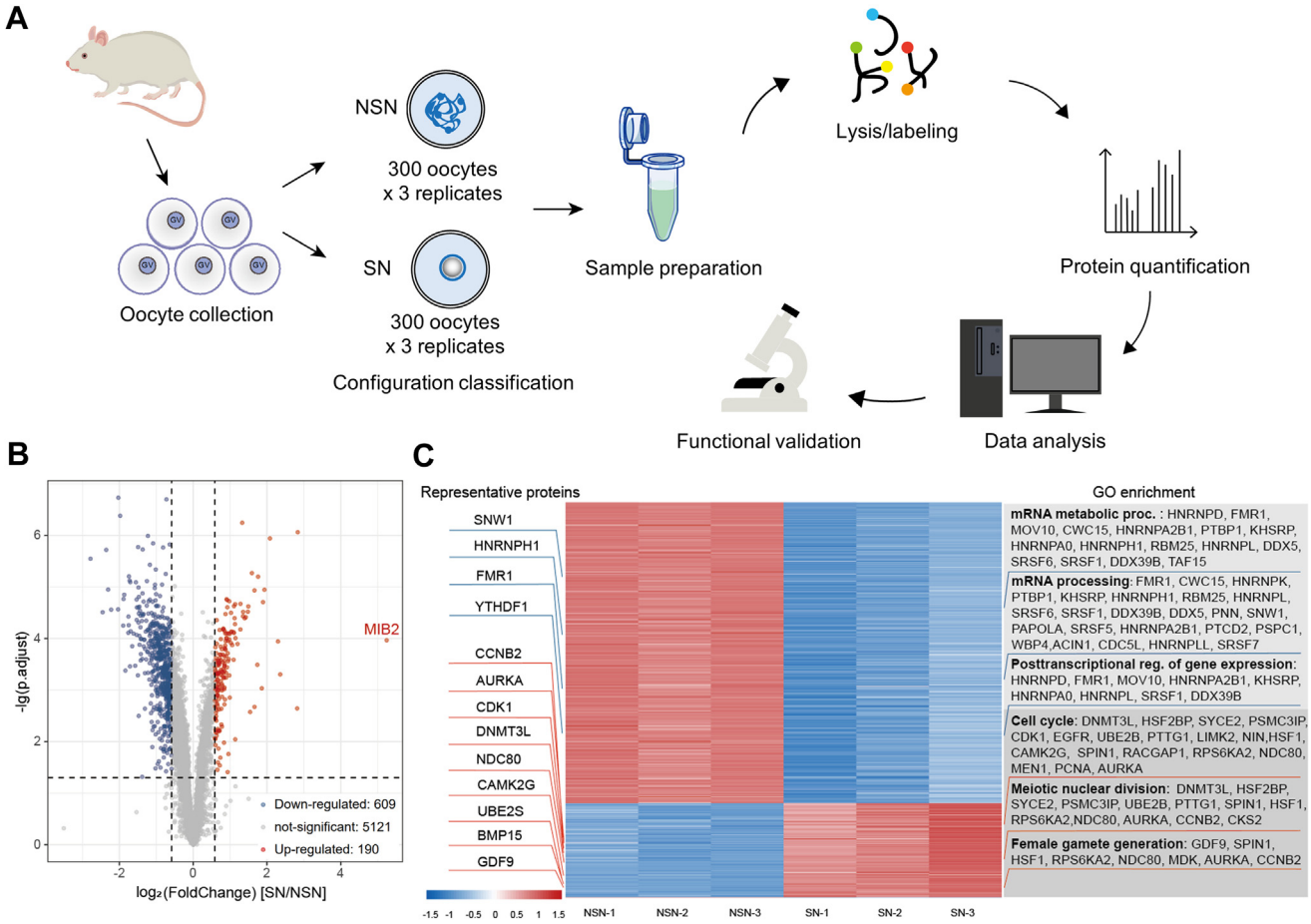

FIG. 1. **Quantitative proteomic analysis unveils MIB2 protein accumulation in SN oocytes**. *A*, schematic overview of the workflow for proteome profiling of mouse oocytes with different chromatin configurations at 3 weeks of age. *B*, Volcano plot analysis of differentially expressed proteins. *Blue dots* represent proteins upregulated in NSN, while *red dots* represent proteins upregulated in SN. *C*, Heatmap of differentially expressed proteins and GO pathway enrichment analysis. In the middle is the heatmap of differentially expressed proteins; on the left are representative downregulated (*blue lines*) and upregulated proteins (*red lines*); on the right are representative enriched pathways for differentially expressed proteins (downregulated protein-enriched pathways in *blue*, upregulated protein-enriched pathways in *red*, p.adjust<0.05, fold change>1.5).

protein ligase 2, SN/NSN = 37.9), which leads us to speculate its role in oocyte configuration transition.

MIB2 Promotes Oocyte Chromatin Configuration Transition

To investigate the function of MIB2, we performed knockdown experiments in SN oocytes and overexpression in NSN oocytes (Fig. 2*A*), assessing its impact on chromatin configuration and transcriptional activity. Firstly, SN oocytes were microinjected with MIB2-targeting siRNA (siMIB2), resulting in a marked reduction of MIB2 protein, as evidenced by western blotting (Fig. 2*B*). Our data indicated that MIB2 knockdown in SN oocytes led to partial chromatin decondensation, exhibiting a configuration similar to NSN (Fig. 2*C*). Furthermore, an increase in the intensities of EU (5-ethynyl uridine) signals in siMIB2 SN oocytes was observed, suggesting a resumption of global transcriptional activity (Fig. 2, *F* and *G*, SN *vs.* SN+siMIB2).

Given the diminished level of MIB2 in NSN oocytes, we subsequently investigated whether enhancing MIB2 contents in NSN oocytes could promote the transition of chromatin configuration. To this end, exogenous *Mib2* mRNA was injected into NSN oocytes, and followed by staining to assess the chromatin configuration. Immunoblotting analysis confirmed that MIB2 protein was effectively overexpressed in NSN oocytes (Fig. 2*D*). As anticipated, overexpression of MIB2 in NSN oocytes led to chromatin condensation and a consequent transition in chromatin configuration from NSN to SN (Fig. 2*E*). Notably, we observed a significant decrease in

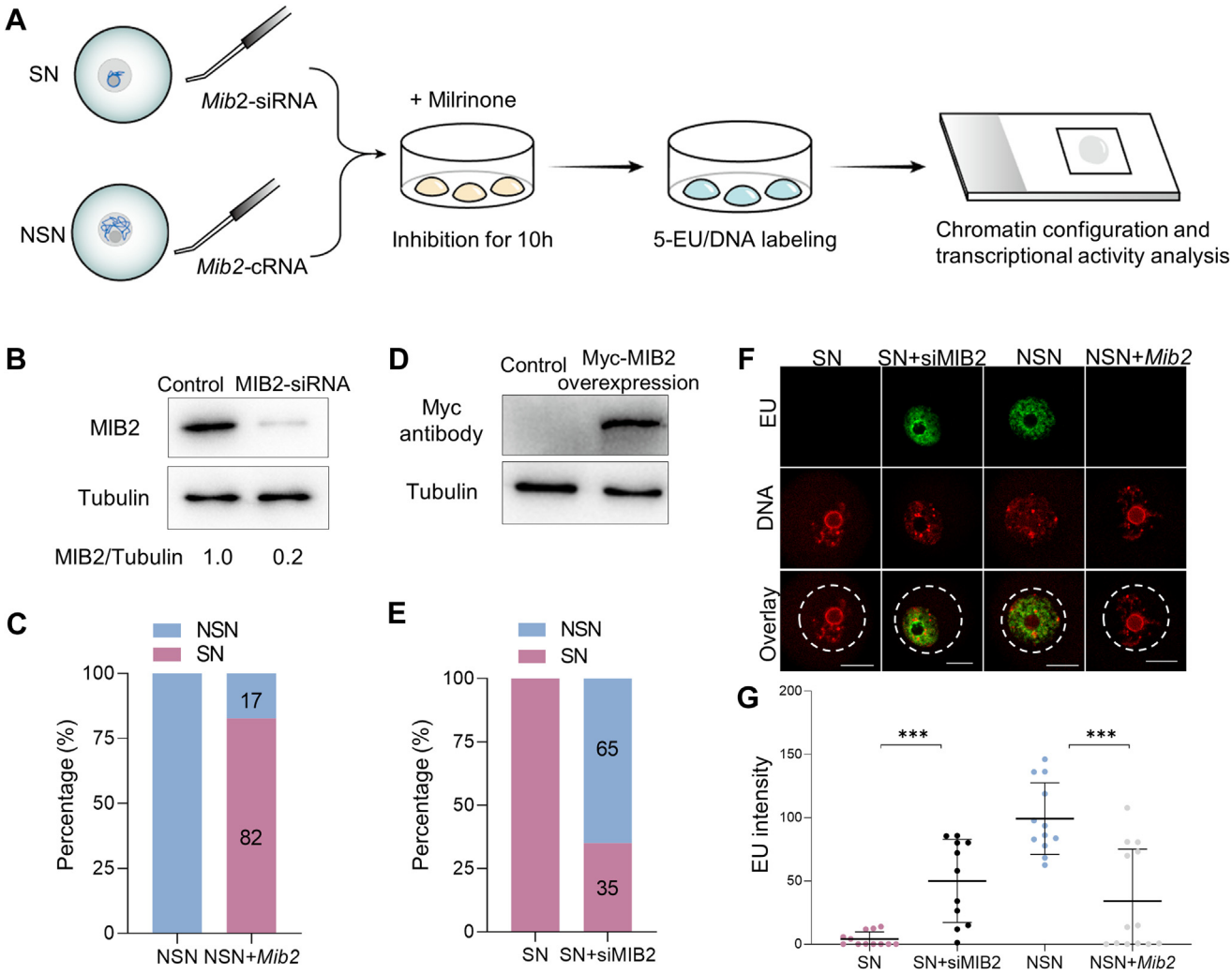

FIG. 2. **MIB2 promotes oocyte chromatin configuration transition**. *A*, a schematic diagram illustrating the functional study of MIB2 in the chromatin configuration of oocytes. *B*, western Blotting to confirm oocyte MIB2 protein depletion. *C*, statistical analysis of the proportion of oocytes with chromatin condensation. The numbers in the columns represent the means. *D*, Western blotting analysis showing that exogenous Myc-MIB2 protein was efficiently overexpressed, probing with anti-Myc antibody. *E*, statistical analysis of the proportion of oocytes with chromatin decondensation. The numbers in the columns represent the means. *F*, representative fluorescence images of oocytes labeled with EU (5-ethynyl uridine). The white dashed circles indicate the areas of transcriptional activity. Scale bar: 10 μm. *G*, statistical analysis of EU signal intensity. Data is represented as mean ± SD. ***$p < 0.001$.

the intensities of EU signals in MIB2 overexpression NSN oocytes, indicating a cessation of global transcriptional activity (Fig. 2, *F* and *G*). Together, these results suggest that MIB2 is essential for oocyte chromatin configuration transition and transcriptional silencing.

MIB2 Functions in Oocyte Meiotic Maturation

A substantial body of research has demonstrated that the chromatin configuration of oocytes is closely associated with their meiotic maturation (32–34). To explore the function of MIB2 in oocyte meiotic maturation, SN oocytes were microinjected with siMIB2. After injections, oocytes were arrested at the GV stage in a medium supplemented with milrinone for 10 h. Subsequently, oocytes were washed in a milrinone-free medium and cultured for 14 h to facilitate the analysis of meiotic maturation (Fig. 3*A*). Only 15.1% of siMIB2 SN oocytes extruded Pb1 (first polar body), significantly lower than that observed in control SN oocytes (71.5%, Fig. 3, *B* and *C*). Correspondingly, the influence of MIB2 on oocyte meiotic maturation also evaluated in NSN oocytes. Our results showed that Pb1 extrusion rates were significantly higher in NSN oocytes with MIB2 overexpression compared with control NSN oocytes (53.1 ± 2.7 *vs.* 34.5 ± 3.0%, Fig. 3, *D* and *E*). Collectively, these findings implied that chromatin configuration transition regulated by MIB2 is crucial for oocyte maturation.

MIB2 is Involved in Spindle Formation and Chromosome Organization

The assembly of the meiotic spindle is critical for the proper chromosome segregation and asymmetric division (35, 36). Considering the fundamental role of MIB2 in oocyte maturation, we then explored whether MIB2 also plays a part in the meiotic apparatus. For this purpose, siMIB2 SN oocytes were immunolabeled with anti-tubulin antibodies to visualize the spindle and simultaneously co-stained with PI for chromosomes. Confocal microscopy coupled with quantitative analysis demonstrated that the majority of SN oocytes exhibited a typical barrel-shaped spindle and well-aligned chromosomes on the metaphase plate. In contrast, the siRNA-mediated MIB2 knockdown in SN oocytes resulted in a markedly increased frequency of abnormal spindle assembly and chromosome organization (Fig. 4, *A* and *B*). Moreover, to further verify if the spindle defects and chromosome misalignment in siMIB2 SN oocytes could lead to the production of aneuploid eggs, we conducted karyotype analysis on Metaphase II (MII) oocytes through chromosome spreading. As depicted in Figure 4, *C* and *D*, aneuploidy was

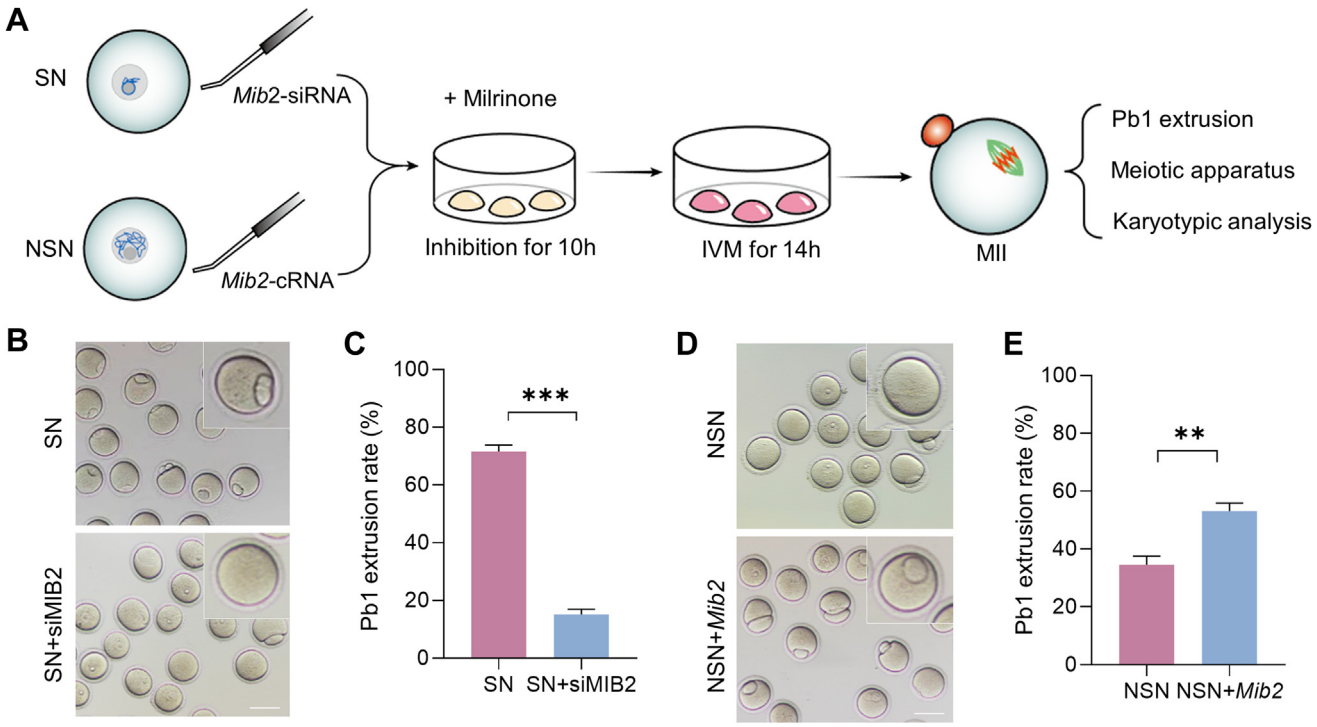

FIG. 3. **MIB2 functions in oocyte meiotic maturation**. *A*, a schematic diagram illustrating the functional study of MIB2 during the meiotic process of oocytes. *B*, DIC images of SN and SN+siMIB2 oocytes at IVM 14 h. The small figure on the *upper right* is a representative oocyte. Scale bar: 80 μm. *C*, statistical analysis of the first polar body extrusion rate. *D*, DIC images of NSN and NSN+*Mib2* oocytes at IVM 14 h. The small figure on the *upper right* is a representative oocyte. Scale bar: 80 μm. *E*, statistical analysis of the first polar body extrusion rate. $^{**}p < 0.01$, $^{***}p < 0.001$.

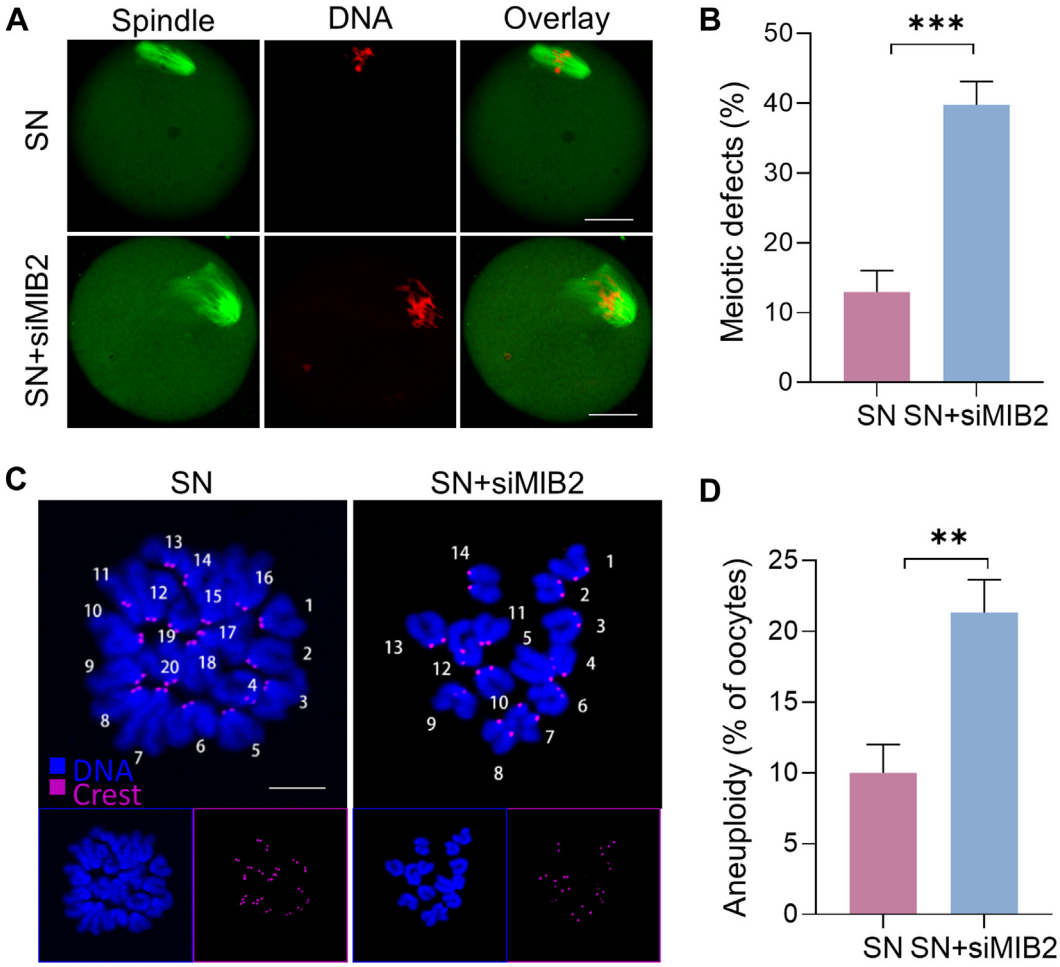

FIG. 4. **MIB2 knockdown causes spindle defects and chromosome misalignment in SN oocytes**. *A*, Immunofluorescence staining of oocyte spindles. α-tubulin (*green*) labels the spindles, and PI (*red*) shows the chromosomes. Scale bar: 25 μm. *B*, statistical analysis of spindle abnormalities in oocytes. *C*, images of oocyte chromatin spreading. CREST (*magenta*) marks kinetochores, and Hoechst-33342 (*blue*) stains the chromosomes. Scale bar: 5 mm. *D*, statistical analysis of the rate of aneuploidy. Data are represented as mean ± SD. $^{**}p < 0.01$, $^{***}p < 0.001$.

observed in 21.3% of siMIB2 SN oocytes, a rate significantly higher compared to control SN oocytes (10%).

To additionally substantiate the functions mentioned above, we conducted overexpression experiments in NSN oocytes aimed at assessing meiotic apparatus. Disorganization of the spindle and failure in chromosome congression were frequently observed in NSN oocytes, as indicated by an arrow in Figure 5*A*. However, the overexpression of MIB2 in NSN oocytes rectified these defects in the meiotic division, mirroring the phenotypes observed in SN oocytes (Fig. 5, *A* and *B*). Significantly, the incidence of non-diploid oocytes was approximately twice as high in NSN oocytes compared to SN oocytes. Concurrently, overexpressing MIB2 in NSN oocytes diminished the occurrence of aneuploidy (Fig. 5, *C* and *D*). Cumulatively, these data indicate that MIB2 is essential for proper spindle assembly and chromosome alignment in oocytes.

MIB2 Enhances the Developmental Competence of Oocytes

The quality of oocytes, also referred to as developmental competence, is pivotal in influencing early embryonic survival, the initiation and continuation of pregnancy, fetal growth, and potentially adult health conditions (37). Developmental competence of oocytes is commonly characterized as the capacity of a female gamete to undergo maturation into an egg, possessing the potential for fertilization and supporting embryonic development up to the blastocyst stage (38). The physiological level of ROS (reactive oxygen species) modulates oocyte functions (39), whereas excessive accumulation results in oxidative stress, directly impairing oocyte quality. Here, we determine whether MIB2 affects oocyte ROS accumulation by CM-H2DCFDA staining. Of note, we found that ROS levels were drastically elevated following MIB2

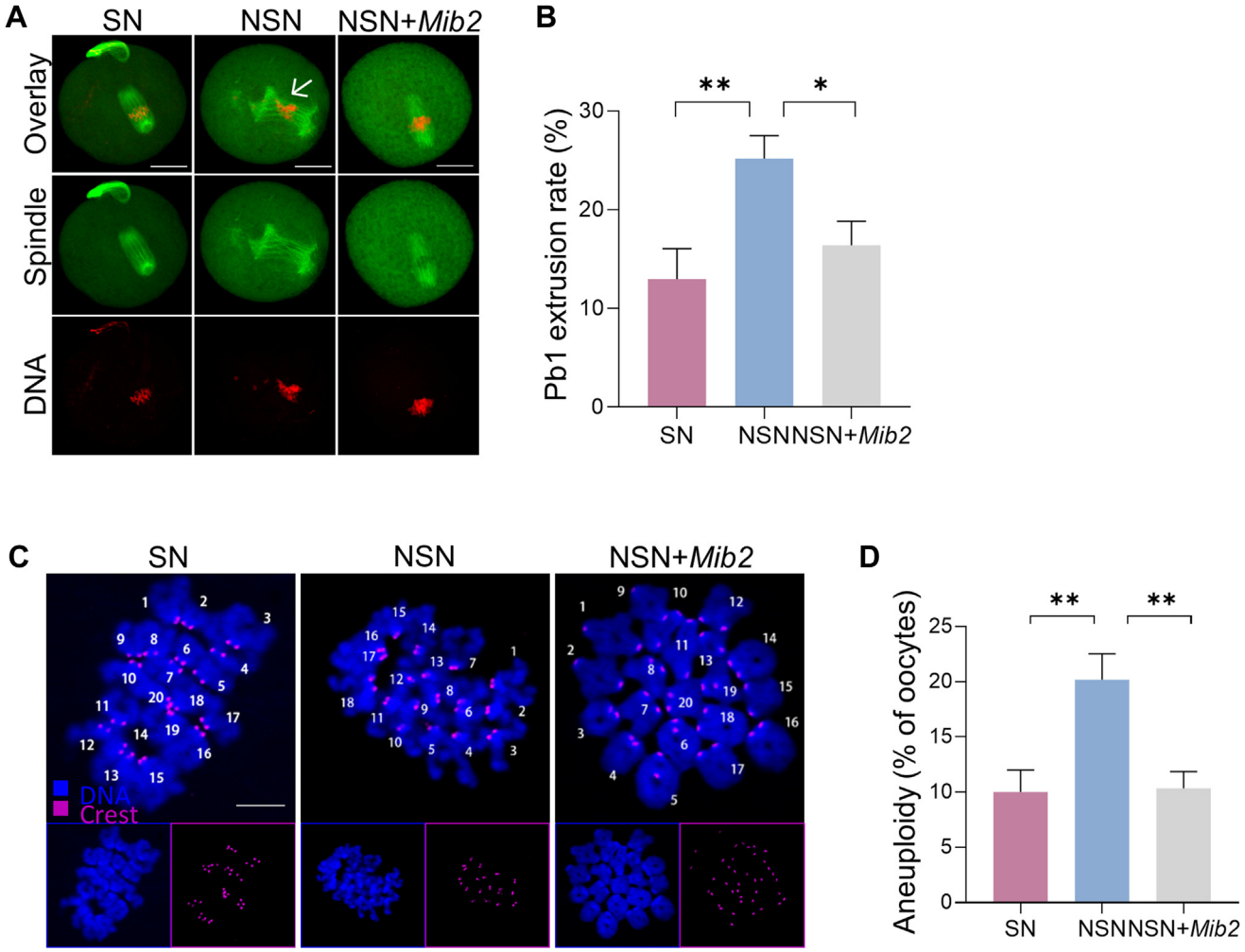

FIG. 5. **MIB2 overexpression partially prevents the meiotic defects in NSN oocytes**. *A*, immunofluorescence staining of oocyte spindles. α-tubulin (*green*) labels the spindles, and PI (*red*) shows the chromosomes. Scale bar: 25 μm. *B*, statistical analysis of spindle abnormalities in oocytes. *C*, images of oocyte chromatin spreading. CREST (*magenta*) marks kinetochores, and Hoechst-33342 (*blue*) stains the chromosomes. Scale bar, 5 mm. *D*, statistical analysis of the rate of aneuploidy. Data is represented as mean ± SD. $^{*}p < 0.05$, $^{**}p < 0.01$.

knockdown in SN oocytes (Fig. 6, *A* and *B*, SN *vs.* SN+si-MIB2). Additionally, we also observed a significant reduction in ROS levels in NSN oocytes with MIB2 overexpression, as compared to control NSN oocytes (Fig. 6, *A* and *B*, NSN *vs.* NSN+*Mib2*).

The disruption of redox homeostasis caused by over-abundant production of ROS may be indicative of diminished quality in oocytes. Hence, we conducted experiments involving parthenogenetic activation and early embryo *in vitro* culture to assess the function of MIB2 in determining the developmental competence of oocytes. Our results demonstrated that the knockdown of MIB2 in SN oocytes markedly decreased the developmental rate of two-cell embryos and hindered their progression to the blastocyst stage (Fig. 6, *C* and *D*, SN *vs.* SN+siMIB2). Conversely, overexpression of MIB2 in NSN oocytes enhanced the development rate to the two-cell embryo stage and facilitated their advancement to the blastocyst stage (Fig. 6, *C* and *D*, NSN *vs.* NSN+*Mib2*). In summary, our findings suggest that MIB2 is pivotal in orchestrating the developmental competence of oocytes.

DISCUSSION

Growing oocytes are highly active in translation and must accumulate high-quality maternal proteins to support subsequent embryonic development (12). Therefore, disturbances in ribosome function and protein metabolism can have profound impacts on oocyte health. Before maturation, mammalian oocytes undergo a transcriptionally and translationally active growth phase, during which essential RNAs, including mRNA and rRNA (40), are synthesized. This is in line with the enriched pathways observed in our proteomic analysis of differentially expressed proteins. The proteomics data show that proteins

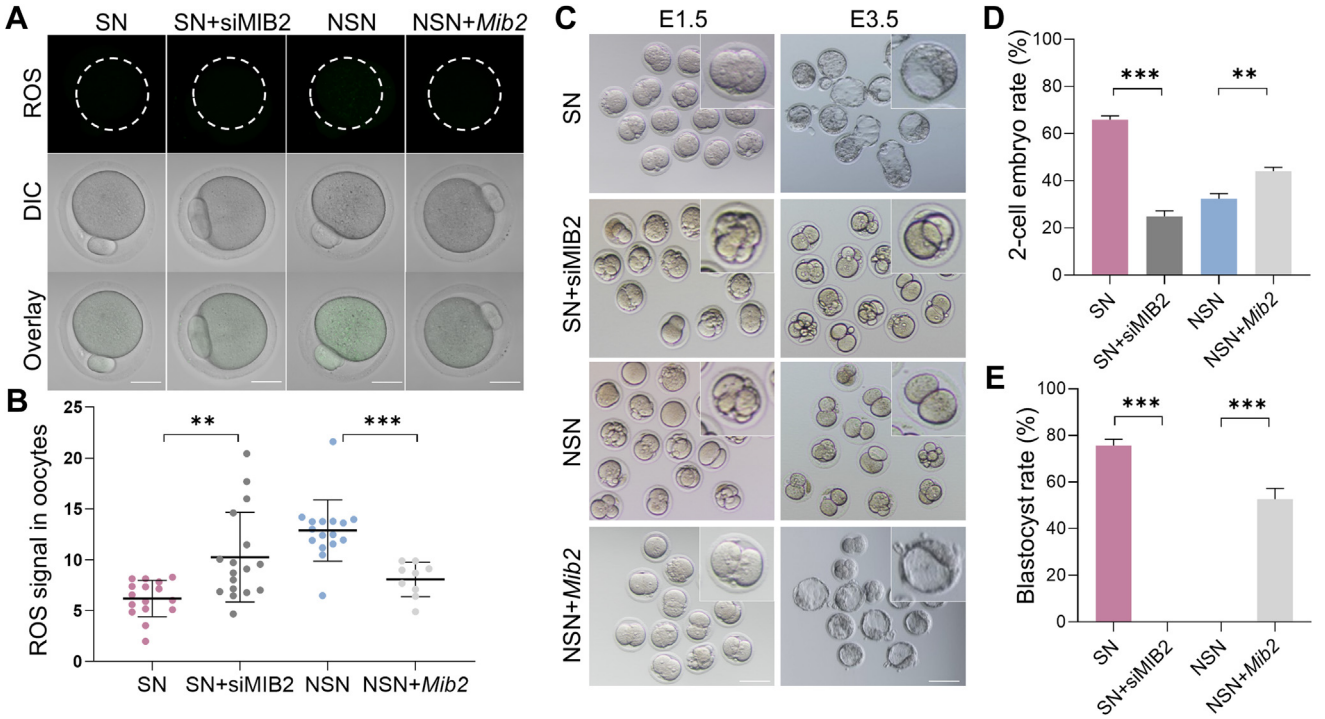

FIG. 6. **MIB2 enhances the developmental competence of oocytes**. *A*, representative images of CM-H2DCFDA fluorescence (*green*) in SN, SN+siMIB2, NSN and NSN+*Mib2* oocytes. Scale bar: 25 μm. The *white dashed circles* represent the cytoplasm of oocytes. *B*, relative ROS levels in SN, SN+siMIB2, NSN and NSN+Mib2 oocytes. Each data point represents an oocyte. *C*, DIC images of SN, NSN, SN+siMIB2, and NSN+Mib2 oocytes at IVM E1.5 and E3.5. The small figure on the *upper right* is a representative oocyte. Scale bar: 80 μm. *D*, Statistical analysis of two-cell embryo development rate, presented as the proportion of two-cell embryos among activated embryos. *E*, statistical analysis of blastocyst development rate, presented as the proportion of blastocysts among two-cell embryos. Data are represented as mean ± SD. $^{**}p < 0.01$, $^{***}p < 0.001$.

upregulated in NSN oocytes are mainly enriched in mRNA metabolic processes and mRNA processing, indicating a significant accumulation of mRNA in immature oocytes. As oocytes grow, RNA synthesis increases dramatically, reaching a peak at the onset of antral follicle formation. At this stage, some oocytes transition to the SN configuration and cease transcription, while others remain in the NSN configuration, maintaining transcriptional activity. The synthesis and storage of transcripts before transcriptional silencing are crucial for oocytes to acquire meiotic competence. Inhibition of oocyte transcriptional activity could lead to defects in subsequent growth and maturation (41). Oocytes that transition from NSN to SN accumulate a large number of proteins related to the cell cycle and meiotic nuclear division. It has been reported that interference with CDK1 activity and failure to accumulate cyclin B1 can impede the progression of meiosis. Additionally, GDF9 and BMP15 are extensively studied for their roles in promoting meiotic maturation (42), thereby enhancing oocyte growth and development.

Just as the timely recruitment of mRNA is crucial for maximum vitality, the proper regulation of protein degradation is also essential. Ubiquitination is closely associated with protein degradation, and the quality of oocytes and embryos depends on the correct processes of protein degradation during maturation. Therefore, ubiquitination plays a significant role in determining the quality of oocytes. For example, the phosphorylation of PATL2 leads to the regulation of PATL2 protein levels through ubiquitin-mediated proteasomal degradation in oocytes, thereby maintaining mRNA stability to ensure proper oocyte maturation and embryonic development (43). Additionally, UBE2S maintains mouse oocyte meiosis by transferring ubiquitin to APC/C (44).

During the late stages of oogenesis, GV oocytes experience chromatin remodeling marked by transcriptional silencing, transitioning from NSN to SN chromatin configuration. This transition is critical for the acquisition of meiotic maturation and developmental competence in oocytes. In our study, it was found that MIB2 is the markedly upregulated protein in SN oocytes in comparison to NSN oocytes, according to quantitative proteomic analysis. This discovery prompted an investigation into the role of MIB2 in the transition of oocyte chromatin configuration. MIB2, an E3 ubiquitin-protein ligase, is recognized for its involvement in Notch signaling. It attenuates TNF-induced apoptosis by ubiquitinating receptor-interacting protein kinase 1 (RIPK1) and cylindromatosis (CYLD) in tumor necrosis factor alpha (TNFα)-induced NF-κB

signaling (45–48). Our research reveals that the knockdown of MIB2 results in increased chromatin de-condensation and associated transcriptional activity. Conversely, MIB2 overexpression leads to heightened chromatin condensation and sustained transcriptional silencing. These observations suggest that MIB2 could potentially regulate the transition of chromatin configuration in oocytes.

Concurrently, the deficiency of MIB2 results in several critical meiosis abnormalities, including reduced rates of Pb1 extrusion, atypical spindle morphology, and chromosomal misalignment (Figs. 3–5). Moreover, these abnormalities contribute to the generation of aneuploidy. These findings collectively highlight the crucial role of MIB2 in regulating meiotic apparatus assembly during oocyte maturation. Defects in chromosomal cohesion, disruption of kinetochore-microtubule (KT-MT) attachment, and spindle assembly checkpoint (SAC) irregularities are key contributors to chromosome missegregation (49, 50). Therefore, we postulate that MIB2 may impact meiosis in multiple aspects.

Low-quality oocytes are a key factor contributing to female pregnancy failure. Common features of low-quality oocytes include abnormalities in the meiotic division apparatus, cytoplasmic heterogeneity, and impaired mitochondrial function. Oxidative stress exerts a toxic effect on oocyte maturation and is considered one of the reasons for the poor quality of oocytes (51, 52). Recent research also indicates that mislocalized MIB2 in oocytes leads to decreased NOTCH2-mediated AKT phosphorylation levels, ultimately compromising oocyte quality (53). Remarkably, proteomic analysis disclosed that more than three-quarters of proteins were found to be downregulated in SN oocytes as compared to NSN oocytes (Fig. 1), indicating potential protein degradation during the transition of oocyte chromatin configuration. MIB2, known for promoting protein degradation *via* ubiquitination, exhibits an upregulation trend that could potentially explain the observed protein degradation. Further research is needed to elucidate the specific molecular mechanisms and signaling pathways by which MIB2 mediates regulatory effects.

In conclusion, various strands of evidence in our study illustrate that MIB2 is pivotal in regulating the transition of oocyte chromatin configuration, meiotic maturation, and development competence of oocytes. These findings suggest a potentially viable strategy to enhance the quality of oocytes and female fertility.

DATA AVAILABILITY

The mass spectrometry proteomics data have been deposited to the ProteomeXchange Consortium *via* the PRIDE (54) partner repository with the dataset identifier PXD048173.

Supplemental Data—This article contains Supplemental data.

Funding and additional information—This work was supported by the National Natural Science Foundation of China (NO. 81925014 and 82221005 to Q. W.; NO. 82101736 to H. S.), the National Key Research and Development Program of China (NO. 2021YFC2700400 to Q. W.) and the Natural Science Foundation of Jiangsu Province (BK20230058 to L. H.).

Author contributions—Y. J., S. Z., and Q. W. conceptualization; Y. J., G. S., J. L., Q. C., H. S., L. H., and X. G. data curation; Y. J. and S. Z. writing–original draft; Y. J., S. Z., and Q. W. writing–review & editing; H. S., L. H., and Q. W. funding acquisition; Q. W. supervision.

Conflict of interest—The authors declare that they have no conflicts of interest with the contents of this article.

Abbreviations—The abbreviations used are: GV, germinal vesicle; GVBD, germinal vesicle breakdown; NSN, non-surrounded nucleolus; SN, surrounded nucleolus.

Received January 10, 2024, and in revised form, June 13, 2024
Published, MCPRO Papers in Press, July 15, 2024, https://doi.org/10.1016/j.mcpro.2024.100813

REFERENCES

1. He, M., Zhang, T., Yang, Y., and Wang, C. (2021) Mechanisms of oocyte maturation and related epigenetic regulation. *Front. Cell Dev. Biol.* **9**, 654028
2. Bennabi, I., Terret, M.-E., and Verlhac, M.-H. (2016) Meiotic spindle assembly and chromosome segregation in oocytes. *J. Cell Biol.* **215**, 611–619
3. Mogessie, B., Scheffler, K., and Schuh, M. (2018) Assembly and positioning of the oocyte meiotic spindle. *Annu. Rev. Cell Dev. Biol.* **34**, 381–403
4. Moor, R. M., D, Y., Lee, C., and Fulka J, J. (1998) Oocyte maturation and embryonic failure. *Hum. Reprod. Update* **4**, 223–236
5. Zhang, Y., Wang, H. H., Wan, X., Xu, Y., Pan, M. H., and Sun, S. C. (2018) Inhibition of protein kinase D disrupts spindle formation and actin assembly during porcine oocyte maturation. *Aging (Albany NY)* **10**, 3736–3744
6. Zeng, J., Jiang, M., Wu, X., Diao, F., Qiu, D., Hou, X., *et al*. (2018) SIRT4 is essential for metabolic control and meiotic structure during mouse oocyte maturation. *Aging Cell* **17**, e12789
7. Wu, Y., Li, M., and Yang, M. (2021) Post-translational modifications in oocyte maturation and embryo development. *Front. Cell Dev. Biol.* **9**, 645318
8. Sun, H., Sun, G., Zhang, H., An, H., Guo, Y., Ge, J., *et al*. (2023) Proteomic profiling reveals the molecular control of oocyte maturation. *Mol. Cell Proteomics* **22**, 100481
9. Sen, A., and Caiazza, F. (2013) Oocyte maturation: a story of arrest and release. *Front. Biosci. (Schol Ed.)* **5**, 451–477
10. De La Fuente, R., Viveiros, M. M., Burns, K. H., Adashi, E. Y., Matzuk, M. M., and Eppig, J. J. (2004) Major chromatin remodeling in the germinal vesicle (GV) of mammalian oocytes is dispensable for global transcriptional silencing but required for centromeric heterochromatin function. *Dev. Biol.* **275**, 447–458
11. Bogolyubova, I., Salimov, D., and Bogolyubov, D. (2023) Chromatin configuration in diplotene mouse and human oocytes during the period of transcriptional activity extinction. *Int. J. Mol. Sci.* **24**, 11517
12. Bouniol-Baly, C., Hamraoui, L., Guibert, J., Beaujean, N., Szöllösi, M. S., and Debey, P. (1999) Differential transcriptional activity associated with chromatin configuration in fully grown mouse germinal vesicle oocytes. *Biol. Reprod.* **60**, 580–587
13. M Zuccotti, A. P., Giorgi Rossi, P., Garagna, S., and Redi, C. A. (1995) Chromatin organization during mouse oocyte growth. *Mol. Reprod. Dev.* **41**, 479–485

14. Lin, J., Chen, F., Sun, M.-J., Zhu, J., Li, Y.-W., Pan, L.-Z., *et al*. (2016) The relationship between apoptosis, chromatin configuration, histone modification and competence of oocytes: a study using the mouse ovary-holding stress model. *Sci. Rep.* **6**, 28347
15. Sui, X., Hu, Y., Ren, C., Cao, Q., Zhou, S., Cao, Y., *et al*. (2020) METTL3-mediated m6A is required for murine oocyte maturation and maternal-to-zygotic transition. *Cell Cycle* **19**, 391–404
16. Inoue, A., Nakajima, R., Nagata, M., and Aoki, F. (2008) Contribution of the oocyte nucleus and cytoplasm to the determination of meiotic and developmental competence in mice. *Hum. Reprod.* **23**, 1377–1384
17. Wang, T., and Na, J. (2021) Fibrillarin-GFP facilitates the identification of meiotic competent oocytes. *Front. Cell Dev. Biol.* **9**, 648331
18. Zuccotti, M., Ponce, R. H., Boiani, M., Guizzardi, S., Govoni, P., Scandroglio, R., *et al*. (2002) The analysis of chromatin organisation allows selection of mouse antral oocytes competent for development to blastocyst. *Zygote* **10**, 73–78
19. Xia, M., He, H., Wang, Y., Liu, M., Zhou, T., Lin, M., *et al*. (2014) PCBP1 is required for maintenance of the transcriptionally silent state in fully grown mouse oocytes. *Cell Cycle* **11**, 2833–2842
20. Zuccotti, M., Merico, V., Sacchi, L., Bellone, M., Brink, T. C., Stefanelli, M., *et al*. (2009) Oct-4 regulates the expression of Stella and Foxj2 at the Nanog locus: implications for the developmental competence of mouse oocytes. *Hum. Reprod.* **24**, 2225–2237
21. Liu, X. M., Yan, M. Q., Ji, S. Y., Sha, Q. Q., Huang, T., Zhao, H., *et al*. (2018) Loss of oocyte Rps26 in mice arrests oocyte growth and causes premature ovarian failure. *Cell Death Dis.* **9**, 1144
22. Pan, L.-Z., Cheng, H., Zhang, J., Gong, S., Tian, X.-D., Pan, C.-J., *et al*. (2021) *In vivo* zearalenone exposure dose-dependently compromises mouse oocyte competence by impairing chromatin configuration and gene transcription. *Reprod. Fertil. Dev.* **33**, 229–238
23. Eleftheriou, K., Peter, A., Fedorenko, I., Schmidt, K., Wossidlo, M., and Arand, J. (2022) A transition phase in late mouse oogenesis impacts DNA methylation of the early embryo. *Commun. Biol.* **5**, 1047
24. Chen, M., Yang, W., Guo, Y., Hou, X., Zhu, S., Sun, H., *et al*. (2023) Multi-omics reveal the metabolic patterns in mouse cumulus cells during oocyte maturation. *J. Ovarian Res.* **16**, 156
25. Wang, H., Zhu, S., Wu, X., Liu, Y., Ge, J., Wang, Q., *et al*. (2021) NAMPT reduction-induced NAD+ insufficiency contributes to the compromised oocyte quality from obese mice. *Aging Cell* **20**, e13496
26. He, Y., Li, X., Gao, M., Liu, H., and Gu, L. (2019) Loss of HDAC3 contributes to meiotic defects in aged oocytes. *Aging Cell* **18**, e13036
27. Feng, S., Li, J., Wen, H., Liu, K., Gui, Y., Wen, Y., *et al*. (2022) hnRNPH1 recruits PTBP2 and SRSF3 to modulate alternative splicing in germ cells. *Nat. Commun.* **13**, 3588
28. Folk, P., Půta, F., and Skružný, M. (2004) Transcriptional coregulator SNW/SKIP: the concealed tie of dissimilar pathways. *Cell Mol. Life Sci.* **61**, 629–640
29. Chen, J., Liao, A., Powers, E. N., Liao, H., Kohlstaedt, L. A., Evans, R., *et al*. (2020) Aurora B-dependent Ndc80 degradation regulates kinetochore composition in meiosis. *Genes Dev.* **34**, 209–225
30. Belli, M., and Shimasaki, S. (2018) Molecular aspects and clinical relevance of GDF9 and BMP15 in ovarian function. *Vitam. Horm.* **107**, 317–348
31. Serpico, A. F., Febbraro, F., Pisauro, C., and Grieco, D. (2022) Compartmentalized control of Cdk1 drives mitotic spindle assembly. *Cell Rep.* **38**, 110305
32. Chalupnikova, K., Solc, P., Sulimenko, V., Sedlacek, R., and Svoboda, P. (2014) An oocyte-specific ELAVL2 isoform is a translational repressor ablated from meiotically competent antral oocytes. *Cell Cycle* **13**, 1187–1200
33. Zhang, J., Zhang, Y. L., Zhao, L. W., Guo, J. X., Yu, J. L., Ji, S. Y., *et al*. (2019) Mammalian nucleolar protein DCAF13 is essential for ovarian follicle maintenance and oocyte growth by mediating rRNA processing. *Cell Death Differ.* **26**, 1251–1266
34. Tan, J. H., Wang, H. L., Sun, X. S., Liu, Y., Sui, H. S., and Zhang, J. (2009) Chromatin configurations in the germinal vesicle of mammalian oocytes. *Mol. Hum. Reprod.* **15**, 1–9
35. Xin, Y., Jin, Y., Ge, J., Huang, Z., Han, L., Li, C., *et al*. (2020) Involvement of SIRT3-GSK3β deacetylation pathway in the effects of maternal diabetes on oocyte meiosis. *Cell Prolif.* **54**, e12940
36. Tilia, L., Venetis, C., Kilani, S., Cooke, S., and Chapman, M. (2016) Is oocyte meiotic spindle morphology associated with embryo ploidy? A prospective cohort study. *Fertil. Steril.* **105**, 1085–e1087
37. Krisher, R. L. (2004) The effect of oocyte quality on development. *J. Anim. Sci.* **82**, E14–E23
38. Conti, M., and Franciosi, F. (2018) Acquisition of oocyte competence to develop as an embryo: integrated nuclear and cytoplasmic events. *Hum. Reprod. Update* **24**, 245–266
39. Prasad, S., Tiwari, M., Pandey, A. N., Shrivastav, T. G., and Chaube, S. K. (2016) Impact of stress on oocyte quality and reproductive outcome. *J. Biomed. Sci.* **23**, 36
40. Kageyama, S., Liu, H., Kaneko, N., Ooga, M., Nagata, M., and Aoki, F. (2007) Alterations in epigenetic modifications during oocyte growth in mice. *Reproduction* **133**, 85–94
41. Ju, J. Q., Pan, Z. N., Zhang, K. H., Ji, Y. M., Liu, J. C., and Sun, S. C. (2023) Mcrs1 regulates G2/M transition and spindle assembly during mouse oocyte meiosis. *EMBO Rep.* **24**, e56273
42. Zhu, J., Yang, Q., Li, H., Wang, Y., Jiang, Y., Wang, H., *et al*. (2022) Sirt3 deficiency accelerates ovarian senescence without affecting spermatogenesis in aging mice. *Free Radic. Biol. Med.* **193**, 511–525
43. Zhang, Z., Liu, R., Zhou, H., Li, Q., Qu, R., Wang, W., *et al*. (2023) PATL2 regulates mRNA homeostasis in oocytes by interacting with EIF4E and CPEB1. *Development* **150**, dev201572
44. Sun, S. M., Zhao, B. W., Li, Y. Y., Liu, H. Y., Xu, Y. H., Yang, X. M., *et al*. (2024) Loss of UBE2S causes meiosis I arrest with normal spindle assembly checkpoint dynamics in mouse oocytes. *Development* **151**, dev202285
45. Feltham, R., Jamal, K., Tenev, T., Liccardi, G., Jaco, I., Domingues, C. M., *et al*. (2018) Mind bomb regulates cell death during TNF signaling by suppressing RIPK1's cytotoxic potential. *Cell Rep.* **23**, 470–484
46. Nakabayashi, O., Takahashi, H., Moriwaki, K., Komazawa-Sakon, S., Ohtake, F., Murai, S., *et al*. (2021) MIND bomb 2 prevents RIPK1 kinase activity-dependent and -independent apoptosis through ubiquitylation of cFLIPL. *Commun. Biol.* **4**, 80
47. Uematsu, A., Kido, K., Takahashi, H., Takahashi, C., Yanagihara, Y., Saeki, N., *et al*. (2019) The E3 ubiquitin ligase MIB2 enhances inflammation by degrading the deubiquitinating enzyme CYLD. *J. Biol. Chem.* **294**, 14135–14148
48. Li, R., Shao, J., Jin, Y.-J., Kawase, H., Ong, Y. T., Troidl, K., *et al*. (2023) Endothelial FAT1 inhibits angiogenesis by controlling YAP/TAZ protein degradation *via* E3 ligase MIB2. *Nat. Commun.* **14**, 1980
49. Lane, S. I., and Jones, K. T. (2014) Non-canonical function of spindle assembly checkpoint proteins after APC activation reduces aneuploidy in mouse oocytes. *Nat. Commun.* **5**, 3444
50. Gruhn, J. R., Zielinska, A. P., Shukla, V., Blanshard, R., Capalbo, A., Cimadomo, D., *et al*. (2019) Chromosome errors in human eggs shape natural fertility over reproductive life span. *Science* **365**, 1466–1469
51. Hu, K. L., Ye, X., Wang, S., and Zhang, D. (2020) Melatonin application in assisted reproductive technology: a systematic review and meta-analysis of randomized trials. *Front. Endocrinol. (Lausanne)* **11**, 160
52. Yu, K., Wang, R. X., Li, M. H., Sun, T. C., Zhou, Y. W., Li, Y. Y., *et al*. (2019) Melatonin reduces androgen production and upregulates heme oxygenase-1 expression in granulosa cells from PCOS patients with hypoestrogenia and hyperandrogenia. *Oxid Med. Cell Longev.* **2019**, 8218650
53. Chen, L.-J., Zhang, N.-N., Zhou, C.-X., Yang, Z.-X., Li, Y.-R., Zhang, T., *et al*. (2021) Gm364 coordinates MIB2/DLL3/Notch2 to regulate female fertility through AKT activation. *Cell Death Differ.* **29**, 366–380
54. Vizcaíno, J. A., Deutsch, E. W., Wang, R., Csordas, A., Reisinger, F., Ríos, D., *et al*. (2014) ProteomeXchange provides globally coordinated proteomics data submission and dissemination. *Nat. Biotechnol.* **32**, 223–226